

# Quantum effects in liquid water: Path-integral simulations of a flexible and polarizable *ab initio* model

Harry A. Stern and B. J. Berne

Department of Chemistry and Center for Biomolecular Simulation, Columbia University, New York, New York 10027

(Received 21 May 2001; accepted 8 August 2001)

We examine quantum effects in liquid water at ambient conditions by performing path-integral molecular dynamics simulations of a flexible, polarizable water model that was parameterized from *ab initio* calculations. The quantum liquid is less structured and has a smaller binding energy, in accord with previous simulations. The difference between the quantum and classical liquid binding energies ( $\sim 1.5$  kcal/mol) is in reasonable agreement with a simple harmonic model, and is somewhat larger than previous estimates in the literature. Quantum effects do not appear to significantly modify the average induced dipole moment for a polarizable model, although the distribution is broader, especially for the component along the  $C_2$  axis of symmetry. © 2001 American Institute of Physics. [DOI: 10.1063/1.1407287]

## I. INTRODUCTION

Methods based on Feynman's path-integral formulation of quantum mechanics<sup>1</sup> have been widely used to calculate finite-temperature equilibrium properties of many-body systems in the condensed phase,<sup>2</sup> including liquid water.<sup>3–6</sup> Kuharski and Rossky performed path-integral Monte Carlo simulations on the rigid, nonpolarizable ST2 model and found that the structural changes due to quantum effects were as large as those due to raising the temperature by  $\sim 50$  K.<sup>4</sup> Wallqvist and Berne performed a study of a central-force model incorporating molecular flexibility and found a similar decrease in hydrogen-bond structure due to quantum effects.<sup>5</sup> Similar results were found for simulations of the SPC model.<sup>7</sup> In addition to computing equilibrium properties, Lobaugh and Voth used the centroid molecular dynamics method to calculate dynamical properties, such as the diffusion constant and Debye dielectric relaxation correlation function, and found them to be faster in the quantum liquid, also consistent with a weaker hydrogen-bond network.<sup>6</sup>

Most path-integral simulations to date have been performed on empirical water models. Since these models are refined by running classical simulations and adjusting the parameters to reproduce experimental liquid properties, they already incorporate quantum effects implicitly. (An exception is the model of Lobaugh and Voth,<sup>6</sup> which was also empirical, but parameterized using quantum simulations.) Path-integral simulations on an *ab initio* potential surface provide a better estimate of quantum effects for the true water potential surface. Much recent simulation work involves forces computed either “on the fly” from quantum-chemical electronic structure calculations—the Car-Parrinello or *ab initio* molecular dynamics method<sup>8–11</sup>—or from analytical potentials derived primarily from such calculations.<sup>12–22</sup> Almost all studies of these potentials have been classical, and for the costlier methods, quantum simulations would be extremely expensive for a system of more than a few molecules. A quantitative comparison of classical and quantum

simulations for at least one *ab initio* potential can clarify the interpretation of classical simulations for other potentials.

## II. METHODS

For the water potential energy we used the flexible, polarizable MCDHO model of Saint-Martin *et al.*<sup>21</sup> This model represents the OH stretch by a Morse function, the HOH bend by a quartic polynomial, and the molecular polarizability by a mobile charge whose position is determined by minimizing the energy for any given atomic configuration. It was fit to high-level *ab initio* calculations of 352 configurations of the water monomer, as well as the geometry and binding energy of the minimum-energy dimer.

All liquid simulations were performed in the canonical (*NVT*) ensemble at 298.15 K and  $0.997$  g/cm<sup>3</sup> with 125 water molecules under cubic boundary conditions. To generate the canonical ensemble, we performed molecular dynamics with a timestep of 0.5 fs using a separate Nosé-Hoover chain thermostat<sup>23–25</sup> for each degree of freedom, 375 thermostat chains in all. Each chain consisted of three thermostats.

Non-electrostatic intermolecular interactions were truncated on a center-of-mass basis at half the box length and a correction to the total energy was applied.<sup>26</sup> All electrostatic interactions were computed using the Ewald sum. In terms of the box length  $L$ , the real-space cutoff was  $c_r = 0.38L$ , the reciprocal-space cutoff was  $c_k = 6.56 \times 2\pi/L$ , and the Ewald screening parameter was set to  $\sqrt{\pi c_k/c_r} \approx 7.36/L$ , the “optimal” value according to the error estimate of Kolafa and Perram.<sup>27</sup>

To check that the liquid properties were reasonably well-converged with respect to the system size and the Ewald parameters, we ran additional classical simulations with larger cutoffs and more molecules; these results are summarized in Table I. Evaluating the potential function requires minimizing the energy with respect to the positions of the mobile charges. We found that minimizing to an accuracy such that the root-mean-square force on the mobile charges

TABLE I. Dependence of liquid binding energy ( $E_{\text{liq}} - E_{\text{gas}}$ ) and average molecular dipole moment ( $\mu$ ) on the number of molecules ( $N$ ) and Ewald cutoffs ( $c_r$ ), the real-space cutoff, expressed in units of the box length  $L$ ; and  $c_k$ , the reciprocal-space cutoff, expressed in units of  $2\pi/L$ . For each set of cutoffs, the screening parameter was set to  $\sqrt{\pi}c_k/c_r$ . The number in parentheses denotes the uncertainty in the last digit.

$N$	$c_r/L$	$c_k L/2\pi$	$E_{\text{liq}} - E_{\text{gas}}$ (kcal/mol)	$\mu$ (D)
125	0.38	7.36	-11.34(2)	2.97(1)
256	0.38	7.36	-11.35(2)	2.97(1)
512	0.38	7.36	-11.24(2)	2.95(1)
125	0.5	7.36	-11.25(3)	2.96(1)
125	0.5	8.0	-11.29(2)	2.96(1)

was 0.01 kcal/(mol Å) led to satisfactory energy conservation and well-converged molecular dipole moments and total system energies, and was not unduly expensive, requiring around seven evaluations of the force on the mobile charges for every time step of molecular dynamics. Less accurate minimization led to drifts in the Nosé-Hoover conserved quantity.

All quantum simulations were performed with the path-integral molecular dynamics (PIMD) method,<sup>2,28</sup> using Nosé-Hoover thermostat chains to generate the canonical ensemble as above. As suggested by Martyna *et al.*,<sup>25</sup> the thermostat masses were set to  $Nk_B T/\omega$  for the first thermostat in the chain and  $k_B T/\omega$  for the other thermostats, where  $\omega$  is a characteristic frequency of the system. Since each thermostat was coupled to only one degree of freedom,  $N=1$  and all thermostats were set to the same frequency. The characteristic frequency was taken to be the frequency of the PIMD harmonic oscillators, that is,  $\omega = \sqrt{P/\beta\hbar}$ , where  $P$  is the number of beads or time slices and  $\beta = 1/k_B T$ .

To check the convergence of our results with respect to  $P$ , we computed the distribution function  $\rho(x)$  for a harmonic oscillator with frequency around that of the OH stretch and mass equal to the reduced mass of hydrogen and oxygen and compared with the exact result,

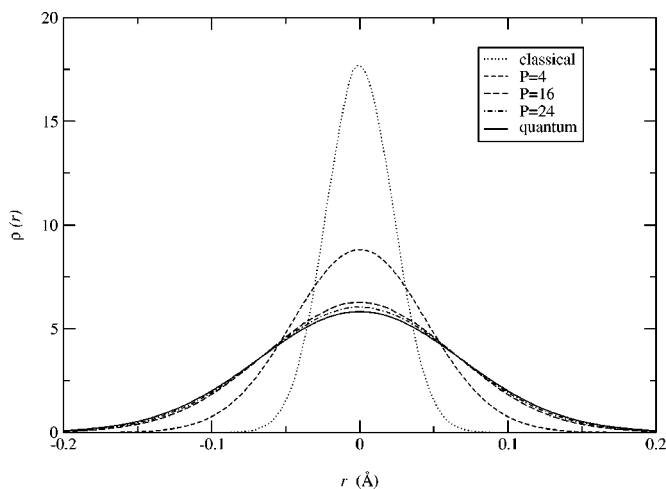


FIG. 1. Position distribution function for a harmonic oscillator in the canonical ensemble at 298.15 K with frequency  $\omega = 716 \text{ ps}^{-1}$  ( $3800 \text{ cm}^{-1}$ , around that of the OH stretch) and mass 0.948 amu. The exact classical and quantum results are shown along with path-integral MD simulations using 4, 16, and 24 beads.

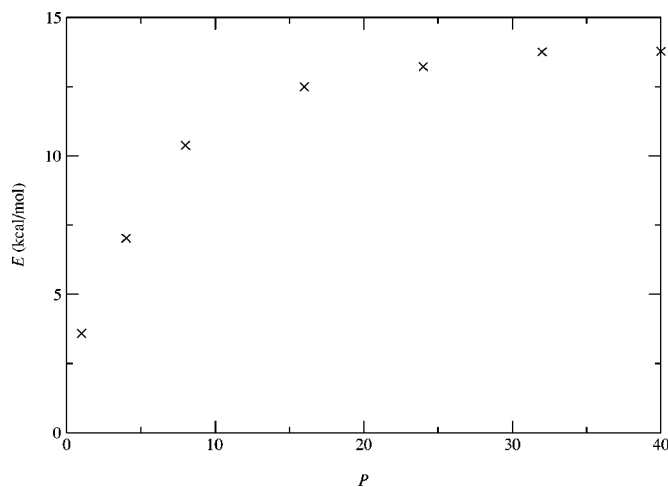


FIG. 2. Energy of an isolated monomer,  $E$ , as a function of the number of beads  $P$  used in a PIMD simulation in the canonical ensemble at 298.15 K.

$$\rho(x) = \sqrt{\frac{\alpha}{\pi}} e^{-\alpha x^2},$$

$$\text{with } \alpha = \begin{cases} \frac{\beta m \omega^2}{2} & (\text{classical}) \\ \frac{m \omega}{\hbar} \tanh \frac{\beta \hbar \omega}{2} & (\text{quantum}). \end{cases} \quad (1)$$

Results are shown in Fig. 1 and indicate that a simulation with  $P=24$  reproduces the quantum distribution function reasonably well. In addition, we computed the energy of an isolated monomer in the canonical ensemble at 298.15 K as a function of  $P$ . The energy of the quantum system is taken as the sum of the potential energy and kinetic energy, where the latter is given by the virial estimator of Herman *et al.*,<sup>29,30</sup>  $K = \langle K_{\text{est}} \rangle$ , with

$$K_{\text{est}} = \frac{1}{2P} \sum_{\alpha=1}^P \sum_{i=1}^N \mathbf{r}_i^\alpha \cdot \nabla_i^\alpha U(\mathbf{r}_1^\alpha, \dots, \mathbf{r}_N^\alpha). \quad (2)$$

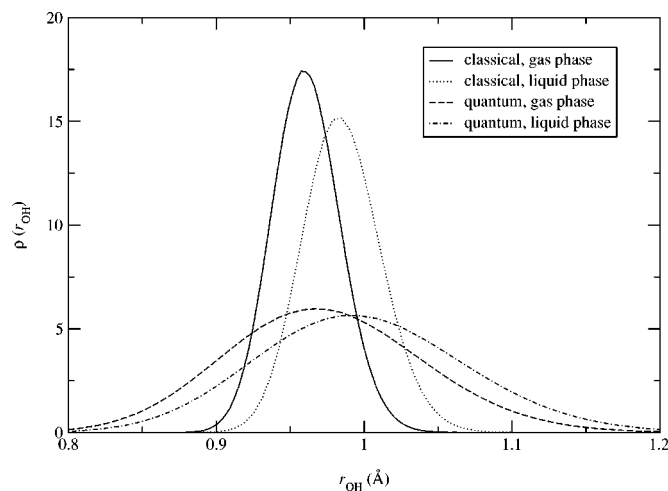


FIG. 3. Distribution of the OH bond length, for classical and quantum simulations, in gas and liquid phase.

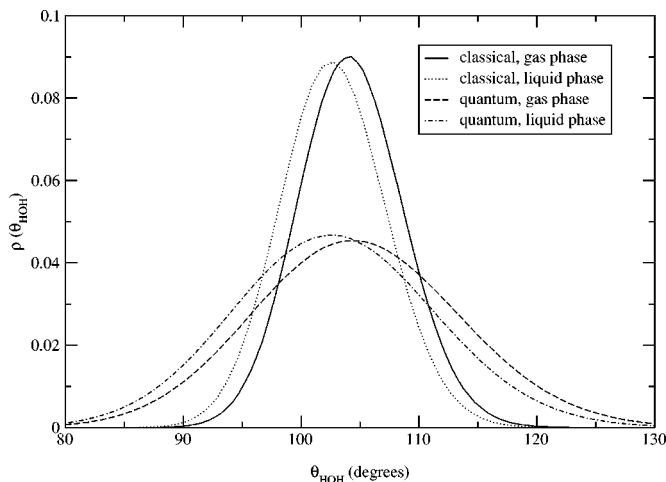


FIG. 4. Distribution of the OH bond angle, for classical and quantum simulations, in gas and liquid phase.

As shown in Fig. 2, the energy is reasonably well converged for  $P = 24$ .

Liquid simulations were equilibrated for at least 100 ps, and equilibrium properties were taken from averages over at least 200 ps of simulation time. Errors were computed using block averaging. Radial distribution functions were computed from a histogram of atomic distances measured only between atoms in the same time slice. The liquid potential energy was taken to be the average potential energy per molecule in the liquid phase minus the average potential energy of an isolated molecule at the same temperature. For a classical simulation, the total binding energy is just the liquid potential energy; the average kinetic energy is the same in gas and liquid phase. For a quantum simulation, the total liquid binding energy is the liquid potential energy plus the difference in average kinetic energies in liquid and gas phase, where these are calculated from the virial estimator of Herman *et al.* as given above.

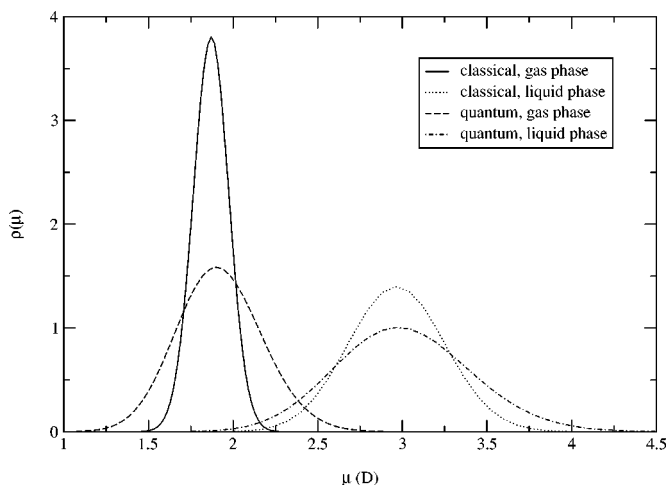


FIG. 5. Distribution of the molecular dipole moment, for classical and quantum simulations, in gas and liquid phase.

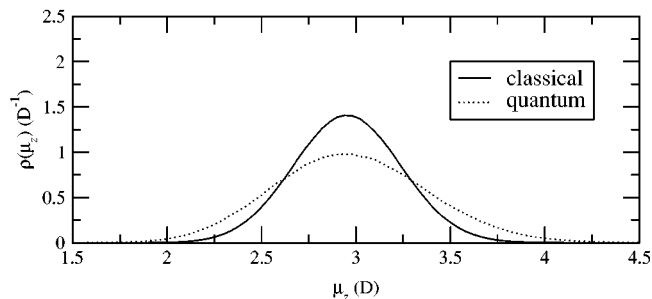
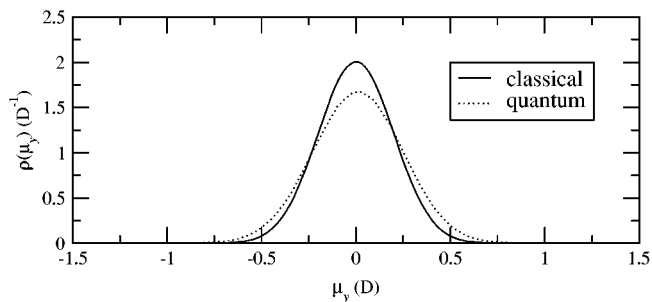
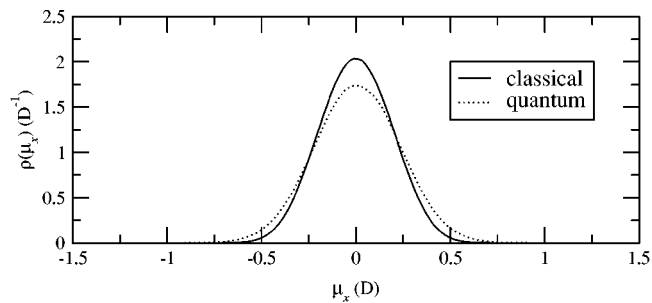


FIG. 6. Distribution of the  $x$ ,  $y$ , and  $z$  components of the molecular dipole moment in liquid phase for classical and quantum simulations.

### III. RESULTS

The distributions of the OH bond length, HOH angle, and molecular dipole moment for classical and quantum simulations, both in gas and liquid phase, are shown in Figs. 3–5. The quantum distributions are broader and shifted slightly towards longer bond lengths and wider angles. For both classical and quantum simulations, the distribution of bond lengths is shifted towards longer bonds in liquid phase, in agreement with recent experimental measurements.<sup>31</sup> However, both classical and quantum simulations show a shift towards smaller HOH angles in the liquid phase, in contrast with the larger angles deduced from experimental measurements of the intramolecular HH distance.<sup>31</sup> This dis-

TABLE II. Gas-phase bond length ( $r_{\text{OH}}$ ), bond angle ( $\theta_{\text{HOH}}$ ), and dipole moment ( $\mu$ ).

	$r_{\text{OH}}$ (Å)	$\theta_{\text{HOH}}$ (degrees)	$\mu$ (D)
Minimum (0 K)	0.9584	104.14	1.861
Classical (298.15 K)	0.9610	104.27	1.869
Quantum (298.15 K)	0.9738	104.81	1.922
Experiment	0.9572 <sup>a</sup>	104.52 <sup>a</sup>	1.855 <sup>b</sup>

<sup>a</sup>Reference 44.

<sup>b</sup>Reference 45.

TABLE III. Liquid-phase average bond length ( $r_{\text{OH}}$ ), average bond angle ( $\theta_{\text{HOH}}$ ), average molecular dipole moment ( $\mu$ ), potential binding energy ( $U_{\text{liq}} - U_{\text{gas}}$ ), and total binding energy ( $E_{\text{liq}} - E_{\text{gas}}$ ), at 298.15 K. The number in parentheses denotes the uncertainty in the last digit.

	$r_{\text{OH}}$ (Å)	$\theta_{\text{HOH}}$ (degrees)	$\mu$ (D)	$U_{\text{liq}} - U_{\text{gas}}$ (kcal/mol)	$E_{\text{liq}} - E_{\text{gas}}$ (kcal/mol)
Classical	0.985	102.79(1)	2.968(5)	-11.34(2)	-11.34(2)
Quantum	0.999	102.91(1)	3.011(3)	-10.89(1)	-9.8(1)
Experiment	0.970 <sup>a</sup>	106(1) <sup>b</sup>	2.9(6) <sup>c</sup>		-9.92 <sup>d</sup>

<sup>a</sup>Reference 31.

<sup>b</sup>From intramolecular OH and HH distances reported in Ref. 31.

<sup>c</sup>Reference 46.

<sup>d</sup>Reference 37.

crepancy appears to be common (if not universal) as the HOH angle for many other flexible water models also grow smaller upon solvation.<sup>6,32-35</sup> It should be noted that an earlier reference<sup>36</sup> reports an experimental angle in the liquid (102.8°) that is also smaller than the gas-phase value and very close to the value predicted by the MCDHO model. The change of the angle upon solvation is likely due to at least two competing effects. Polarization from surrounding molecules induces a larger dipole moment and thus should be associated with a smaller angle. But the constraint of (partial) tetrahedral ordering should induce a larger angle closer to the tetrahedral angle, 109.47°.

The quantum distribution of the molecular dipole moment is broader than the classical distribution, but the average is not significantly different from that given by the classical distribution (it is larger by 0.04 D). This contrasts with the simulations of flexible models of Lobaugh and Voth,<sup>6</sup> who found smaller dipole moments in quantum simulations. This discrepancy can be understood as follows. Quantization results in weaker intermolecular interactions, so we expect that water molecules are not as strongly polarized—this accounts for the smaller dipole moments observed by Lobaugh and Voth. However, the present model uses a Morse potential for the OH stretch and therefore experiences a shift towards larger OH bond lengths (and thus larger dipole moments) upon including quantum effects. For the present model, the effects of weaker intermolecular interactions and quantization of a Morse potential nearly cancel as the average dipole moment is essentially unchanged. However, the model used by Lobaugh and Voth used a harmonic potential for the OH stretch, which does not have a shift towards larger bond lengths upon quantization. Thus the effects of weaker intermolecular interactions are not counteracted, and they observe a smaller dipole moment. (The HOH angle also changes upon quantization, but only by a fraction of a degree, so the effect on the dipole moment is negligible.)

The distribution of each component of the dipole moment in the liquid phase is shown in Fig. 6. Here the coordinate axes are oriented such that the water molecule lies in the  $yz$  plane, with the  $z$  axis along the  $C_2$  axis of symmetry. (The  $x$  axis then points out of the plane of the molecule and the  $y$  axis points in the direction of the vector connecting the two hydrogens.) The quantum distributions are slightly wider than the classical distributions; the difference between classical and quantum distributions is more pronounced for the component along the  $C_2$  axis than for the other components.

Energetic results for gas- and liquid-phase simulations are summarized in Tables II and III. The quantum result for the liquid binding energy, 9.8 kcal/mol, is quite close to the experimental value, 9.92 kcal/mol, which was taken from the heat of vaporization under the assumption that the gas is ideal and the pressure-volume contribution to the enthalpy is negligible in the liquid.<sup>37,38</sup> The difference in liquid binding energies between quantum and classical simulations is 1.5 kcal/mol. This is larger than previous estimates in the literature, which have ranged from 0.2 kcal/mol<sup>39</sup> to 1.34 kcal/mol.<sup>14</sup>

The difference between quantum and classical energies was compared with a simple approximation, wherein the system is treated as a collection of coupled harmonic oscillators whose spectral density  $g(\omega)$  is computed from the Fourier transform of the velocity autocorrelation function:<sup>40</sup>

$$g(\omega) \propto \int_{-\infty}^{\infty} \sum_n \langle \mathbf{v}_n(0) \cdot \mathbf{v}_n(t) \rangle e^{i\omega t} dt. \quad (3)$$

Here  $\mathbf{v}_n(t)$  is the velocity of atom  $n$  at time  $t$  and the sum is taken over all atoms  $n$ .

For the liquid, the velocity autocorrelation function was computed from five classical molecular dynamics trajectories of 50 ps, each of which was started from a configuration sampled from the canonical ensemble. The spectral density  $g_{\text{liq}}(\omega)$  is normalized such that

$$\int_0^{\infty} g_{\text{liq}}(\omega) d\omega = 9N - 3, \quad (4)$$

the number of degrees of freedom for a liquid of  $N$  flexible water molecules under periodic boundary conditions. (The center of mass is fixed, removing three degrees of freedom from the original  $9N$  atomic coordinates; however, the system is free to undergo net rotations, so that there are  $9N - 3$  degrees of freedom rather than  $9N - 6$  as there would be in a crystal with both center of mass and orientation fixed.)

For the gas, the vibrational spectral density  $g_{\text{gas}}(\omega)$  was computed from the velocity autocorrelation function of an ensemble of trajectories of isolated molecules with no net angular or linear momentum and with initial relative velocities and positions sampled from the Boltzmann distribution, and normalized such that

$$\int_0^{\infty} g_{\text{gas}}(\omega) d\omega = 3N, \quad (5)$$

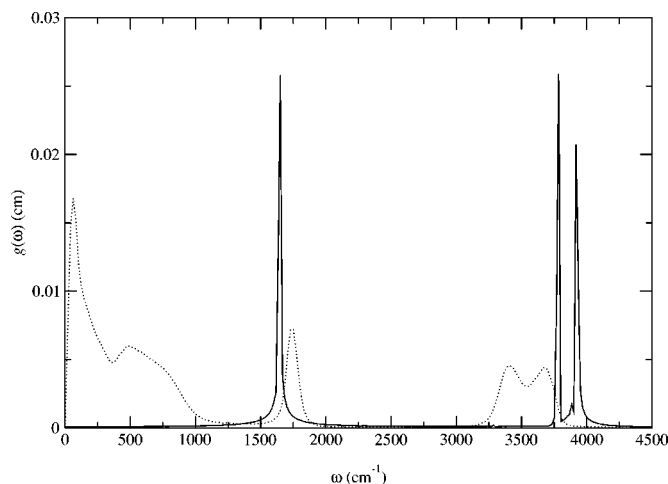


FIG. 7. Spectral density of liquid MCDHO water (dotted line), and vibrational spectral density of gas-phase MCDHO water (solid line).

the number of vibrational degrees of freedom.

The spectral densities for both gas and liquid are shown in Fig. 7. The peaks in the gas and liquid spectra corresponding to the stretch and bend frequencies are given and compared with experimental frequencies from neutron-scattering spectroscopy<sup>41</sup> in Table IV. Both stretch and bend frequencies are somewhat too high. In comparing the liquid to the gas, we observe a blueshift in the HOH bend and a redshift of the OH stretch, in accord with experiment. The magnitude of the shift of the bend frequency agrees reasonably well with experiment, but that of the stretch frequency is overestimated.

The quantum correction to the classical liquid-phase energy is then given by the difference in energies between a collection of quantum oscillators in the canonical ensemble with mode density  $g_{\text{liq}}(\omega)$  and a collection of classical oscillators:

$$\Delta E_{\text{liq}} = \frac{1}{N} \int_0^\infty \left[ g_{\text{liq}}(\omega) \left( \frac{\hbar\omega}{2} \coth \frac{\beta\hbar\omega}{2} \right) - k_B T \right] d\omega. \quad (6)$$

An analogous correction was computed for the gas. The quantum correction consists of a rotational and vibrational contribution:  $\Delta E_{\text{gas}} = \Delta E_{\text{gas}}^{\text{rot}} + \Delta E_{\text{gas}}^{\text{vib}}$ . The rotational contribution was computed from the difference between the aver-

TABLE IV. Vibrational frequencies of water in gas and liquid phase. All frequencies are in  $\text{cm}^{-1}$ .

	Bend	Symmetric stretch	Antisymmetric stretch
$\omega_{\text{gas}}$ (MCDHO model)	1651	3785	3918
$\omega_{\text{gas}}$ (experiment) <sup>a</sup>	1595	3657	3756
$\omega_{\text{liq}}$ (MCDHO model)	1740	3407	3668
$\omega_{\text{liq}}$ (experiment) <sup>b</sup>	1670		3557
$\omega_{\text{liq}} - \omega_{\text{gas}}$ (MCDHO model)	89	-378	-250
$\omega_{\text{liq}} - \omega_{\text{gas}}$ (experiment)	75		-150

<sup>a</sup>Reference 47.

<sup>b</sup>Reference 41.

TABLE V. Differences between energies of quantum simulations and classical simulations, for gas phase and liquid phase, as given by PIMD simulations and a harmonic-oscillator model. All energies are in kcal/mol.

	$\Delta E_{\text{liq}}$	$\Delta E_{\text{gas}}$	$\Delta E_{\text{liq}} - \Delta E_{\text{gas}}$
PIMD	11.2	9.7	1.5
Harmonic model	12.1	10.4	1.7

age energy of a quantum asymmetric top<sup>42</sup> and  $3k_B T/2$ . The vibrational contribution was computed from Eq. (6) by substituting  $g_{\text{gas}}(\omega)$  for  $g_{\text{liq}}(\omega)$ .

The quantum corrections are summarized in Table V. For both gas and liquid phase, the difference between quantum and classical systems given by the harmonic model is somewhat larger than that calculated from the simulations. This is expected as the true potential is anharmonic, which lowers the zero-point energy. However, there is cancellation of error in gas and liquid phase, and the net correction to the liquid binding energy, 1.7 kcal/mol, is in good agreement with the difference between the PIMD and classical liquid binding energies, 1.5 kcal/mol.

We may divide the correction to the liquid-phase energy into intramolecular and intermolecular contributions by splitting the integral over the liquid-phase spectral density in Eq. (6) into two regions. Motions with frequencies below  $1200 \text{ cm}^{-1}$  correspond primarily to librations, while those with frequencies above  $1200 \text{ cm}^{-1}$  correspond primarily to intramolecular stretches and bends, so we may write  $\Delta E_{\text{liq}} = \Delta E_{\text{liq}}^{\text{intra}} + \Delta E_{\text{liq}}^{\text{inter}}$ , where

$$\Delta E_{\text{liq}}^{\text{intra}} = \frac{1}{N} \int_{\omega_c}^\infty \left[ g_{\text{liq}}(\omega) \left( \frac{\hbar\omega}{2} \coth \frac{\beta\hbar\omega}{2} \right) - k_B T \right] d\omega \quad (7)$$

$$\Delta E_{\text{liq}}^{\text{inter}} = \frac{1}{N} \int_0^{\omega_c} \left[ g_{\text{liq}}(\omega) \left( \frac{\hbar\omega}{2} \coth \frac{\beta\hbar\omega}{2} \right) - k_B T \right] d\omega, \quad (8)$$

and  $\omega_c = 1200 \text{ cm}^{-1}$ . (The magnitudes of  $\Delta E_{\text{liq}}^{\text{intra}}$  and  $\Delta E_{\text{liq}}^{\text{inter}}$  are insensitive to the exact value of  $\omega_c$  as long as it lies in the region of very low spectral density between the highest frequencies corresponding to librations and the lowest frequencies corresponding to bends.) These contributions, along with the rotational and vibrational contributions to the correction to the gas-phase energy defined above, are shown in Table VI. The net correction to the liquid binding energy,  $\Delta E_{\text{liq}} - \Delta E_{\text{gas}} \approx 1.7 \text{ kcal/mol}$ , is due to two competing effects: a positive contribution due to zero-point energy of in-

TABLE VI. Contributions to the gas- and liquid-phase quantum corrections to the average energy as given by a simple harmonic-oscillator model. All energies are expressed in kcal/mol.

$\Delta E_{\text{liq}}^{\text{inter}}$	2.0	$\Delta E_{\text{gas}}^{\text{rot}}$	-0.3	$\Delta E_{\text{liq}}^{\text{inter}} - \Delta E_{\text{gas}}^{\text{rot}}$	2.3
$\Delta E_{\text{liq}}^{\text{intra}}$	10.1	$\Delta E_{\text{gas}}^{\text{vib}}$	10.7	$\Delta E_{\text{liq}}^{\text{intra}} - \Delta E_{\text{gas}}^{\text{vib}}$	-0.6
$\Delta E_{\text{liq}}$	12.1	$\Delta E_{\text{gas}}$	10.4	$\Delta E_{\text{liq}} - \Delta E_{\text{gas}}$	1.7

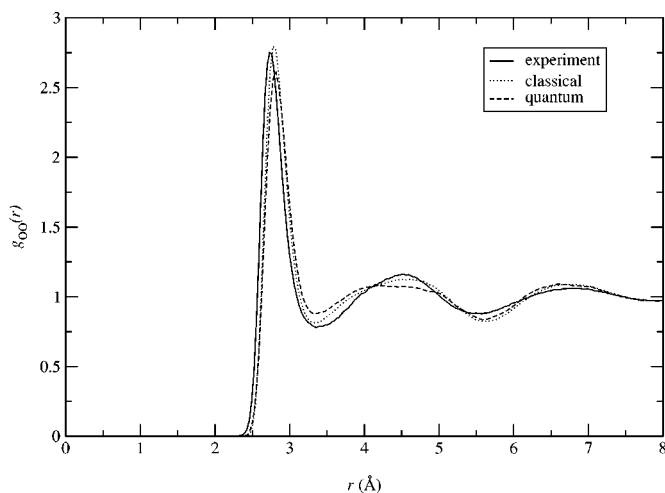


FIG. 8. OO radial distribution function for classical and quantum simulations along with experimental results from Soper.

termolecular librations that are not present (or correspond to free rotations and translations) in the gas phase, and a negative contribution from smaller intramolecular zero-point energy in liquid phase compared with gas phase, due primarily to the redshifting of the OH stretch.

Radial distribution functions are shown in Figs. 8–10 along with the most recent experimental results from the Soper lab.<sup>43</sup> In agreement with previous studies, the peak heights and depths are smaller and shifted towards slightly larger distances for the quantum liquid than for the classical liquid, indicating more disorder in the hydrogen-bond network. There is close agreement between the quantum simulations and experiment in the intramolecular region, while the classical simulations show discrepancies, indicating that quantum effects are important to correctly describe the intramolecular water geometry, and that the intramolecular potential seems to be of high quality. Agreement between quantum simulations and experiment is not as good for the intermolecular structure, indicating that the intermolecular

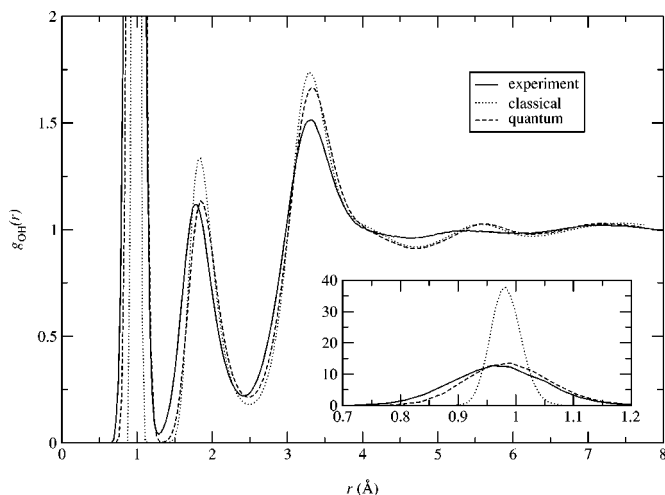


FIG. 9. OH radial distribution function for classical and quantum simulations along with experimental results from Soper. Inset graphs show close-ups of the intramolecular region.

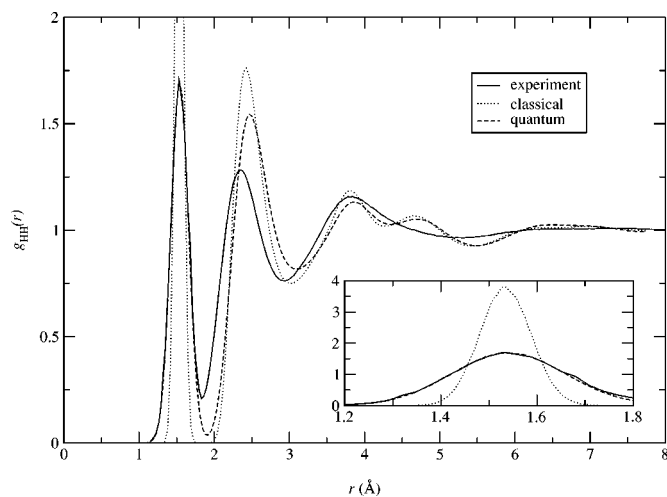


FIG. 10. HH radial distribution function for classical and quantum simulations along with experimental results from Soper. Inset graphs show close-ups of the intramolecular region.

potential energy surface could be improved, as was remarked upon in the MCDHO paper.<sup>21</sup> It should be noted that the experimental radial distribution functions are calculated under the assumption that the structure is isotope-independent.

#### IV. CONCLUSIONS

We have examined quantum effects in liquid water at ambient conditions by running path-integral molecular dynamics simulations of a flexible, polarizable water model that was parameterized from *ab initio* calculations. Including quantum effects results in a less structured hydrogen-bond network and a less tightly bound liquid, in agreement with previous studies. The difference between the quantum and classical liquid binding energies ( $\sim 1.5$  kcal/mol) is larger than previous estimates in the literature, and is in reasonable agreement with a simple harmonic model. The harmonic model suggests that quantum effects on the liquid binding energy are due to two competing contributions: a positive contribution due to zero-point energy of intermolecular librations and vibrations not present in the gas phase, and a negative contribution due to redshifting of the highest intramolecular vibrational frequencies, i.e., the OH stretch.

The MCDHO potential gives a good description of the intramolecular structure in the liquid, although the bond angle is slightly too small; however, the intermolecular potential appears to be of somewhat lesser quality. Quantum effects do not appear to significantly modify the average induced dipole moment for a polarizable water model, although the distribution of dipole moments is wider, especially for the component along the  $C_2$  axis. It would be interesting to extend this work by comparing other equilibrium properties such as the dielectric constant or heat capacity (these properties were not computed in the present study because they are much slower to converge, as they are calculated from fluctuations rather than averages), in addition to dynamical properties via an approximate quantum dynamics method such as centroid molecular dynamics.

## ACKNOWLEDGMENT

This work was supported by Grant No. CHE-00-76279 from the National Science Foundation.

- <sup>1</sup>R. P. Feynman and A. R. Hibbs, *Quantum Mechanics and Path Integrals* (McGraw-Hill, New York, 1965).
- <sup>2</sup>B. J. Berne and D. Thirumalai, *Annu. Rev. Phys. Chem.* **37**, 401 (1986).
- <sup>3</sup>R. A. Kuharski and P. J. Rossky, *Chem. Phys. Lett.* **103**, 357 (1984).
- <sup>4</sup>R. A. Kuharski and P. J. Rossky, *J. Chem. Phys.* **82**, 5164 (1985).
- <sup>5</sup>A. Wallqvist and B. J. Berne, *Chem. Phys. Lett.* **117**, 214 (1985).
- <sup>6</sup>J. Lobaugh and G. A. Voth, *J. Chem. Phys.* **106**, 2400 (1997).
- <sup>7</sup>G. S. del Buono, P. J. Rossky, and J. Schnitker, *J. Chem. Phys.* **95**, 3728 (1991).
- <sup>8</sup>R. Car and M. Parrinello, *Phys. Rev. Lett.* **55**, 2471 (1985).
- <sup>9</sup>K. Laasonen, M. Sprik, M. Parrinello, and R. Car, *J. Chem. Phys.* **99**, 9080 (1993).
- <sup>10</sup>P. L. Silvestrelli, M. Bernasconi, and M. Parrinello, *Chem. Phys. Lett.* **277**, 478 (1997).
- <sup>11</sup>M. Diraison, G. J. Martyna, and M. E. Tuckerman, *J. Chem. Phys.* **111**, 1096 (1999).
- <sup>12</sup>G. C. Lie, E. Clementi, and M. Yoshimine, *J. Chem. Phys.* **64**, 2314 (1976).
- <sup>13</sup>O. Matsuoka, E. Clementi, and M. Yoshimine, *J. Chem. Phys.* **64**, 1351 (1976).
- <sup>14</sup>G. C. Lie and E. Clementi, *Phys. Rev. A* **33**, 2679 (1986).
- <sup>15</sup>U. Niesar, G. Corongiu, E. Clementi, G. R. Kneller, and D. K. Bhattacharya, *J. Phys. Chem.* **94**, 7949 (1990).
- <sup>16</sup>C. Millot and A. J. Stone, *Mol. Phys.* **77**, 439 (1992).
- <sup>17</sup>P.-O. Åstrand, P. Linse, and G. Karlström, *Chem. Phys.* **191**, 195 (1995).
- <sup>18</sup>E. M. Mas, K. Szalewicz, R. Bukowski, and B. Jeziorski, *J. Chem. Phys.* **107**, 4207 (1997).
- <sup>19</sup>Y.-P. Liu, K. Kim, B. J. Berne, R. A. Friesner, and S. W. Rick, *J. Chem. Phys.* **108**, 4739 (1998).
- <sup>20</sup>C. Millot, J.-C. Soetens, M. T. C. M. Costa, M. P. Hodges, and A. J. Stone, *J. Phys. Chem. A* **102**, 754 (1998).
- <sup>21</sup>H. Saint-Martin, J. Hernández-Cobos, M. I. Bernal-Uruchurtu, I. Ortega-Blake, and H. J. C. Berendsen, *J. Chem. Phys.* **113**, 10 899 (2000).
- <sup>22</sup>H. A. Stern, F. Rittner, B. J. Berne, and R. A. Friesner, *J. Chem. Phys.* **115**, 2237 (2001).
- <sup>23</sup>S. Nosé, *Mol. Phys.* **52**, 255 (1984).
- <sup>24</sup>W. G. Hoover, *Phys. Rev. A* **31**, 1695 (1985).
- <sup>25</sup>G. J. Martyna, M. L. Klein, and M. E. Tuckerman, *J. Chem. Phys.* **97**, 2635 (1992).
- <sup>26</sup>M. P. Allen and D. J. Tildesley, *Computer Simulation of Liquids* (Clarendon, Oxford, 1987).
- <sup>27</sup>J. Kolafa and J. W. Perram, *Mol. Simul.* **9**, 351 (1992).
- <sup>28</sup>M. E. Tuckerman, B. J. Berne, G. J. Martyna, and M. L. Klein, *J. Chem. Phys.* **99**, 2796 (1993).
- <sup>29</sup>M. F. Herman, E. J. Bruskin, and B. J. Berne, *J. Chem. Phys.* **76**, 5150 (1982).
- <sup>30</sup>J. Cao and B. J. Berne, *J. Chem. Phys.* **91**, 6359 (1989).
- <sup>31</sup>K. Ichikawa, Y. Kameda, T. Yamaguchi, H. Wakita, and M. Misawa, *Mol. Phys.* **73**, 79 (1991).
- <sup>32</sup>A. Wallqvist, *Chem. Phys.* **148**, 439 (1990).
- <sup>33</sup>J.-L. Barrat and I. R. McDonald, *Mol. Phys.* **70**, 535 (1990).
- <sup>34</sup>S.-B. Zhu, S. Yao, J.-B. Zhu, S. Singh, and G. W. Robinson, *J. Phys. Chem.* **95**, 6211 (1991).
- <sup>35</sup>G. Corongiu, *Int. J. Quantum Chem.* **42**, 1209 (1992).
- <sup>36</sup>W. E. Thiessen and A. M. Narten, *J. Chem. Phys.* **77**, 2656 (1982).
- <sup>37</sup>G. S. Kell, *J. Chem. Eng. Data* **20**, 97 (1975).
- <sup>38</sup>W. L. Jorgensen, J. Chandrasekhar, J. D. Madura, R. W. Impey, and M. L. Klein, *J. Chem. Phys.* **79**, 926 (1983).
- <sup>39</sup>J. C. Owicki and H. A. Scheraga, *J. Am. Chem. Soc.* **99**, 7403 (1977).
- <sup>40</sup>P. H. Berens, D. H. J. Mackey, G. M. White, and K. R. Wilson, *J. Chem. Phys.* **79**, 2375 (1983).
- <sup>41</sup>S.-H. Chen, K. Toukan, C.-K. Loong, D. L. Price, and J. Teixeira, *Phys. Rev. Lett.* **53**, 1360 (1984).
- <sup>42</sup>R. N. Zare, *Angular Momentum* (Wiley, New York, 1988).
- <sup>43</sup>A. K. Soper, *Chem. Phys.* **258**, 121 (2000).
- <sup>44</sup>W. S. Benedict, N. Gailar, and E. K. Phylar, *J. Chem. Phys.* **24**, 1139 (1956).
- <sup>45</sup>S. A. Clough, Y. Beers, G. P. Klein, and L. S. Rothman, *J. Chem. Phys.* **59**, 2254 (1973).
- <sup>46</sup>Y. S. Badyal, M.-L. Saboungi, D. L. Price, S. D. Shastri, D. R. Haefner, and A. K. Soper, *J. Chem. Phys.* **112**, 9206 (2000).
- <sup>47</sup>G. Herzberg, *Electronic Spectra and Electronic Structure of Polyatomic Molecules* (Van Nostrand Reinhold, New York, 1966).